# Desired Dynamics-Based Generalized Inverse Solver for Estimation Problems


### *Authors:*

Shaojie Liu, Yulong Zhang, Zhiqiang Gao, Yangquan Chen, Donghai Li, Min Zhu



*Date Submitted:* 2023-02-20

*Keywords:* generalized inverse, desired dynamics, error-correction mechanism, estimator, disturbance observer, extended state observer



*Abstract:*

An important task for estimators is to solve the inverse. However, as the designs of different estimators for solving the inverse vary widely, it is difficult for engineers to be familiar with all of their properties and to design suitable estimators for different situations. Therefore, we propose a more structurally unified and functionally diverse estimator, called generalized inverse solver (GIS). GIS is inspired by the desired dynamics of control systems and understanding of the generalized inverse. It is similar to a closed-loop system, structurally consisting of nominal models and an error-correction mechanism (ECM). The nominal models can be model-based, semi-model-based, or even model-free, depending on prior knowledge of the system. In addition, we design the ECM of GIS based on desired dynamics parameterization by following a simple and meaningful rule, where states are directly used in the ECM to accelerate the convergence of GIS. A case study considering a rotary flexible link shows that GIS can greatly improve the noise suppression performance with lower loss of dynamic estimation performance, when compared with other common observers at the same design bandwidth. Moreover, the dynamic estimation performances of the three GIS approaches (i.e., model-based, semi-model-based, and model-free) are almost the same under the same parameters. These results demonstrate the strong robustness of GIS (although by means of the uniform design method). Finally, some control cases are studied, including a comparison with DOB and ESO, in order to illustrate their approximate equivalence to GIS.



*Record Type:* Published Article

*Submitted To:* LAPSE (Living Archive for Process Systems Engineering)

| | |
|---|---|
| *Citation (overall record, always the latest version):* | LAPSE:2023.0718 |
| *Citation (this specific file, latest version):* | LAPSE:2023.0718-1 |
| *Citation (this specific file, this version):* | LAPSE:2023.0718-1v1 |

*DOI of Published Version:* https://doi.org/10.3390/pr10112193



*License:* Creative Commons Attribution 4.0 International (CC BY 4.0)

processes

MDPI

*Article*

# Desired Dynamics-Based Generalized Inverse Solver for Estimation Problems

**Shaojie Liu [1], Yulong Zhang [2], Zhiqiang Gao [3], Yangquan Chen [4], Donghai Li [1,*] and Min Zhu [5]**

[1] State Key Laboratory of Power Systems, Department of Energy and Power Engineering, Tsinghua University, Beijing 100084, China
[2] School of Mathematics and Statistics, MIIT Key Laboratory of Mathematical Theory and Computation in Information Security, Beijing Institute of Technology, Beijing 100081, China
[3] Center for Advanced Control Technologies, Cleveland State University, Cleveland, OH 44115, USA
[4] Mechatronics, Embedded Systems and Automation (MESA) Lab, School of Engineering, University of California, Merced, CA 95343, USA
[5] Key Laboratory for Thermal Science and Power Engineering of Ministry of Education, Department of Energy and Power Engineering, Tsinghua University, Beijing 100084, China
* Correspondence: lidongh@tsinghua.edu.cn

**Abstract:** An important task for estimators is to solve the inverse. However, as the designs of different estimators for solving the inverse vary widely, it is difficult for engineers to be familiar with all of their properties and to design suitable estimators for different situations. Therefore, we propose a more structurally unified and functionally diverse estimator, called generalized inverse solver (GIS). GIS is inspired by the desired dynamics of control systems and understanding of the generalized inverse. It is similar to a closed-loop system, structurally consisting of nominal models and an error-correction mechanism (ECM). The nominal models can be model-based, semi-model-based, or even model-free, depending on prior knowledge of the system. In addition, we design the ECM of GIS based on desired dynamics parameterization by following a simple and meaningful rule, where states are directly used in the ECM to accelerate the convergence of GIS. A case study considering a rotary flexible link shows that GIS can greatly improve the noise suppression performance with lower loss of dynamic estimation performance, when compared with other common observers at the same design bandwidth. Moreover, the dynamic estimation performances of the three GIS approaches (i.e., model-based, semi-model-based, and model-free) are almost the same under the same parameters. These results demonstrate the strong robustness of GIS (although by means of the uniform design method). Finally, some control cases are studied, including a comparison with DOB and ESO, in order to illustrate their approximate equivalence to GIS.

**Keywords:** generalized inverse; desired dynamics; error-correction mechanism; estimator; disturbance observer; extended state observer

check for updates

**Citation:** Liu, S.; Zhang, Y.; Gao, Z.; Chen, Y.; Li, D.; Zhu, M. Desired Dynamics-Based Generalized Inverse Solver for Estimation Problems. *Processes* **2022**, *10*, 2193. https://doi.org/10.3390/pr10112193

Academic Editor: Jie Zhang

Received: 24 September 2022
Accepted: 19 October 2022
Published: 26 October 2022

**Publisher's Note:** MDPI stays neutral with regard to jurisdictional claims in published maps and institutional affiliations.

**Copyright:** © 2022 by the authors. Licensee MDPI, Basel, Switzerland. This article is an open access article distributed under the terms and conditions of the Creative Commons Attribution (CC BY) license (https://creativecommons.org/licenses/by/4.0/).

## 1. Introduction

Estimation algorithms are required to process incomplete and imperfect information provided by the sensors, thereby allowing for reconstruction of a reliable estimate of the whole system state in the case where not all state variables are directly measurable [1,2]. Thus, the estimator plays a decisive and crucial role for decision-making, control, measurement, and detection applications, among others. A very important task of estimators is to solve the inverse; for example, solving the inverse of the system, finding the derivatives of each order of the system, and obtaining the disturbances can all be achieved by solving the inverse. In terms of control, several common observer types with this function are the full-state observer (FSO) [3], disturbance observer (DOB) [4], extended state observer (ESO) [5], high-gain observer (HGO) [6,7], and so on.

In practical engineering, it is often necessary to design estimators based on a prior knowledge of the system, hardware conditions, and the engineering domain knowledge.

However, the design principles of different estimators mentioned above vary widely. It is difficult for engineers to be familiar with all of their properties and to design a suitable estimator. Therefore, a practical estimator that is structurally unified and functionally interchangeable is urgently required. This estimator should have such characteristics that it should follow the same approach structurally even in different cases, and it must be capable of being adjusted functionally to different model information and estimation requirements.

For this, we first further review the basic principles of common observers for estimating the inverse. FSO has a long history, the most representative of which is the Luenberger observer (LO) [8,9]. More complex structures were later derived for different systems and application situations, such as nonlinear systems [10,11], networks [12,13], and chaotic systems [14]. Regardless of which FSO is involved, almost all information of the model is used. Therefore, it is dependent on the detailed model of the system and, thus, is less robust. Even though the DOB is somewhat robust in the case of model perturbation, it has a single function and a cumbersome design process for non-minimum phase systems [15,16], as it directly solves the inverse of nominal model. ESO does not depend on a detailed model [17,18]. The total disturbances are estimated by continuous integration of the estimation error; hence, its ability to estimate is limited. HGO also does not depend on a specific model [19,20], but uses a single function and does not make good use of the model information, when available. Some scholars have also been interested in comparing the performance among different estimators [1,21–23], such as LO, HGO, sliding-mode observers, robust state estimator, and ESO. Furthermore, studies combining different algorithms to solve the same problem have also been presented, such as the DOB and Kalman filter (KF) for motion [24], HGO and ESO for a quadrotor [25], KF and DOB for DFIG [26], and mixed estimators [27,28], among others.

After extensive theoretical and applied research on various types of observers, we propose a more structurally unified and functionally diverse estimator, called generalized inverse solver (GIS). GIS is inspired by the desired dynamics of control systems and understanding of the generalized inverse. The generalized inverse enables various estimation functions. GIS is an estimator that is structurally similar to a closed-loop system, consisting of nominal models and an error-correction mechanism (ECM). Specifically, the nominal model can be model-based, semi-model-based, or even model-free depending on the prior knowledge of the model information. In addition, we design pole placement for the ECM of GIS, based on desired dynamics-based parameterization [5,29], where states are directly used in ECM to accelerate convergence of GIS. The dynamics of the GIS are assigned through desired dynamic equation proportional-integral-derivative (DDE PID) control [29–32], which eventually tunes the dynamics of GIS to more standardized desired dynamics by following a simple rule. The behavior of GIS is easier to analyze based on these desired dynamics, and this method of desired dynamics-based parameterization is easy to tune and physically meaningful. In addition, GIS builds a bridge through which the functional transformation between different observers can be realized. We then conducted a case study, which shows that GIS can greatly improve the noise suppression performance with little losses of dynamic estimation performance. Moreover, different GISs can be designed, according to the amount of knowledge of the system model. The dynamic estimation performance of these different GISs is almost the same, illustrating the strong robustness of GISs(although by means of the uniform design method). Finally, some control cases are studied, including a comparison with DOB and ESO to illustrate their approximate equivalence with GIS. Assuming the same knowledge of the system, GIS is compared with DOB and ESO to estimate the performance of the system, both separately and in the control loop.

Focusing on above problems, the paper provides the following contributions:

(1) A novel estimator, named generalized inverse solver (GIS), which is more structurally unified and functionally diverse, is presented. Using GIS to solve the generalized inverse, many estimation problems can be solved; for example, solving the inverse

of the system, finding the derivatives of each order of the system, and obtaining the disturbances.

(2) A desired dynamics-based parameterization method is proposed to correct the estimation error of GIS, where states are directly used in the error-correction mechanism (ECM) to accelerate the convergence of GIS. This method is simple and physically meaningful, called desired dynamics-based GIS. Besides, the nominal models in GIS can be model-based, semi-model-based, or even model-free depending on prior knowledge of the system.

(3) Case studies of rotary flexible link are presented through the simulation, in order to test the performance of GIS in comparison with that of other observers. Some control cases are studied, including a comparison with DOB and ESO, in order to illustrate their approximate equivalence with GIS.

The reminder of this paper is organized as follows: Section 2 further clarifies the research issues. Section 3 introduces the basic idea and structure of GIS. Section 4 presents three asymptotic properties under Assumption 3. A desired dynamics-based parameterization is proposed in Section 5 , which is used to tune the ECM of GIS. The stability of GIS is proven under Theorem 1 in Section 6. Case studies of GIS, in order to test and compare its performance with that of common estimators, are detailed in Section 7. Some discussions and conclusions are provided in Section 8. Finally, Appendix A details the fundamentals of DDE PID. Appendix B gives the proof of Theorem 1. Appendix C provides the proof for Corollary 1 of Theorem 1.

## 2. Problem Formulation

Observers work by combining the knowledge of the system, the control signal $u$, and the output signal $y$ , providing an estimate superior to that which can be obtained when using a feedback device alone. As shown in Figure 1, the observer augments the sensor outputs and provides feedback signals $y_c$, such as the disturbance, inverse, and derivatives. $d$ in Figure 1 represents the lumped disturbances and their estimate. Undoubtedly, $y$ and $u$ are necessary for observers. The requirement of knowledge regarding the system varies from observer to observer, as mentioned in Section 1.

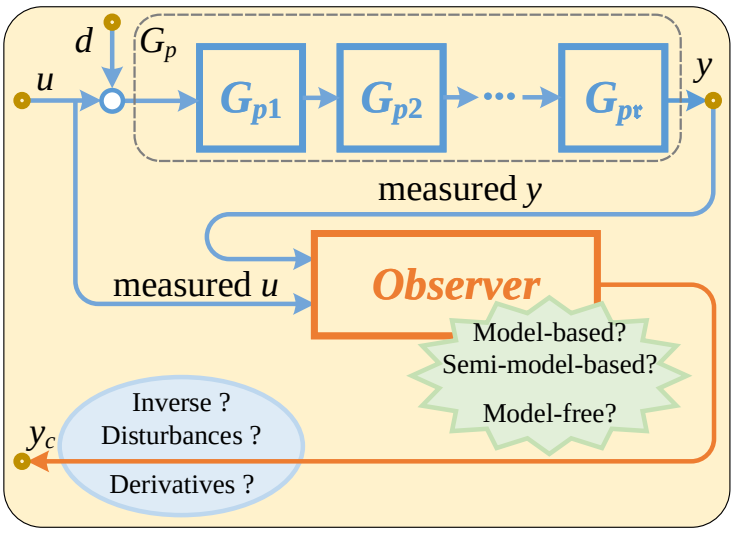


**Figure 1.** The observer problem.

As mentioned in [29], a single-input single-output process can be depicted as a general system, as follows:

$$\frac{\hat{y}}{\hat{u}} = G_p(s) := \mathfrak{H}\frac{\beta(s)}{\alpha(s)} \equiv \mathfrak{H}\frac{\sum_{i=0}^{\mathfrak{n}-\mathfrak{r}} \beta_i s^i}{\sum_{i=0}^{\mathfrak{n}} \alpha_i s^i}, \quad \alpha_{\mathfrak{n}} \equiv 1, \beta_{\mathfrak{n}-\mathfrak{r}} \equiv 1, \tag{1}$$

where $\mathfrak{n}$, $\mathfrak{r}$, and $\mathfrak{H}$ are defined as the order of denominator, the relative degree, and the high frequency gain, respectively; the symbol $s$ denotes Laplace operator; and the notation $\hat{\divideontimes}$ indicates using the Laplace transform for $\divideontimes$, that is, $\hat{\divideontimes} = \mathfrak{L}(\divideontimes)$. Note that coefficients $\alpha_i (i = 1, 2, \ldots, \mathfrak{n}-1)$, $\beta_j (j = 1, 2, \ldots, \mathfrak{n}-\mathfrak{r}-1)$, and $\mathfrak{H}$ are usually unknown.

**Assumption 1.** *The numerator and the denominator of the transfer function $G_p(s)$ are relative primes, and the unobservable and uncontrollable modes are asymptotically stable*

Under Assumption 1, a minimal realization of (1) can be given in terms of a triplet $\sum(A, B, C)$:

$$\begin{aligned} \dot{x} &= Ax + Bu, \\ y &= Cx, \end{aligned} \tag{2}$$

where $x$ represents the state vector of system (1). More generally, an accurate model of (2) is almost unavailable. A nominal model is expressed as $\sum(A_n, B_n, C_n)$, whose frequency domain representation is $G_n$. A common observer of $\sum(A_n, B_n, C_n)$ can be designed as:

$$\begin{aligned} \dot{x}_e &= A_n x_e + B_n u + L(y - y_e), \\ y_e &= C_n x_e, \end{aligned} \tag{3}$$

where $L$ means the observer gain, and $x_e$ and $y_e$ are the estimate state vector and estimate output vector, respectively. ESO is a special case of (3) when the nominal model is of the integral series type (i.e., $G_n = \frac{1}{s^{\mathfrak{r}}}$). The total disturbance estimated by ESO is written as:

$$\tilde{f} = \beta_{\mathfrak{r}+1} \int (y - y_e) dt, \tag{4}$$

where $\beta_{\mathfrak{r}+1}$ is the extend observer gain. Moreover, it is well-known that a DOB can estimate the disturbance precisely if it stays within the bandwidth of the DOB's low-pass filter $Q$ ([4,15]). The disturbance estimated by the DOB is expressed as:

$$\hat{\tilde{d}} = Q(G_n^{-1}\hat{y} - \hat{u}), \tag{5}$$

It is obvious, from (4) that ESO is a model-free or model-independent method, while DOB is based on finding the inverse of $G_n$. The higher the precision of the inverse, the more accurate the disturbance estimate. Therefore, ESO and DOB represent two extreme examples of perturbation estimation. There are many scenarios in practical engineering where nominal models have low accuracy, such as when nominal models are constructed when knowing only information such as the cutoff frequency or time scale of the system. Here, we call such methods semi-model-based. This is the estimation problem encountered in the vast majority of practical scenarios.

The aim of this paper is to design a solver adaptable to different knowledge of the system, called generalized inverse solver (GIS). We divide it into three types: Model-based, semi-model-based, and model-free. If we have an accurate model a priori, GIS takes the accurate model as the nominal model. If we only have an approximate model, GIS can be designed based on the approximate model. If no model knowledge is known, GIS considers the integral series model as the nominal model. Note that we hope that, no matter which type of model information is assumed, a unified and simple tuning method can be used. In addition, disturbance, inverses, and derivatives are estimated simultaneously, once the GIS parameters are tuned.

## 3. Fundamentals of General Estimator

It can be seen, from Figure 2a, that GIS mainly contains two parts—the error-correction mechanism $E$ and nominal model $G_n$, combining blocks in cascade from $G_{n1}$ to $G_{nm}$, where $m$ denotes the relative order of $G_n$. The error-correction mechanism $E$ mainly aims to tune the desired dynamics of GIS. GIS is intended to estimate the inverse, derivatives, and

disturbances, which depends on the design requirements of the control system and prior knowledge of the nominal model. $y_c$, shown in Figure 2a, is the controlled output vector with respect to time, consisting of $y_{e1}$ to $y_{em}$ (the estimated values of the corresponding intermediate variables) and $\tilde{f}$ (the disturbance); that is,

$$y_c \coloneqq (y_{e1}, y_{e2}, y_{e3}, \ldots, y_{e(m-1)}, y_{em}, \tilde{f})^\top. \tag{6}$$

$y_v$ represents the virtual measured output vector versus time, consisting of $y_{e1}$ to $y_{em}$; that is,

$$y_v \coloneqq (y_{v1}, y_{v2}, y_{v3}, \ldots, y_{v(m-1)}, y_{vm})^\top. \tag{7}$$

GIS, as an estimator, is usually arranged in the loop (see Figure 2b). The inputs of GIS are measured or are available variables $y$ and $u$. The input–output relationships of GIS are expressed as:

$$\begin{aligned} \begin{pmatrix} \hat{y}_c \\ \hat{y}_v \end{pmatrix} &=: G\hat{u}_e - G_3\hat{u} \\ &=: \underbrace{\begin{pmatrix} G_1 \\ G_2 \end{pmatrix}}_{G} \underbrace{\overbrace{\begin{pmatrix} E_F & -E_B \end{pmatrix}}^{E} \begin{pmatrix} \hat{y} \\ \hat{y}_v \end{pmatrix}}_{u_e} - G_3\hat{u}, \end{aligned} \tag{8}$$

where $G$ and $E$ denote the transfer matrices of the generalized system and the ECM, respectively. The three sub-matrices of $G$, $G_1$ $G_2$, and $G_3$ , are expressed as:

$$G_1 = T_1 \begin{pmatrix} G_{nm} \ldots G_{n2}G_{n1} \\ G_{n(m-1)} \ldots G_{n2}G_{n1} \\ G_{n(m-2)} \ldots G_{n2}G_{n1} \\ \vdots \\ G_{n2}G_{n1} \\ G_{n1} \\ 1 \end{pmatrix}_{(m+1)\times 1}, G_2 = T_2 \begin{pmatrix} G_{nm} \ldots G_{n2}G_{n1} \\ G_{n(m-1)} \ldots G_{n2}G_{n1} \\ G_{n(m-2)} \ldots G_{n2}G_{n1} \\ \vdots \\ G_{n2}G_{n1} \\ G_{n1} \end{pmatrix}_{m\times 1}, G_3 = \begin{pmatrix} \left.\begin{matrix} 0 \\ \vdots \\ 0 \end{matrix}\right\} m \\ 1 \\ \left.\begin{matrix} 0 \\ \vdots \\ 0 \end{matrix}\right\} m \end{pmatrix}_{(2m+1)\times 1}, \tag{9}$$

where $T_1$ and $T_2$ are transformation matrices. Generally, $T_1$ is an identity matrix, and $T_2$ is a diagonal matrix.

$$T_2 = \begin{pmatrix} 1 & 0 & 0 & \ldots & 0 & 0 \\ 0 & sG_{nm} & 0 & \ldots & 0 & 0 \\ 0 & 0 & s^2G_{nm}G_{n(m-1)} & \ldots & 0 & 0 \\ \vdots & \vdots & \vdots & \ddots & \vdots & \vdots \\ 0 & 0 & 0 & \ldots & s^{(m-2)}G_{nm}G_{n(m-1)} \ldots G_3 & 0 \\ 0 & 0 & 0 & \ldots & 0 & s^{(m-1)}G_{nm}G_{n(m-1)} \ldots G_2 \end{pmatrix}_{m\times m}. \tag{10}$$

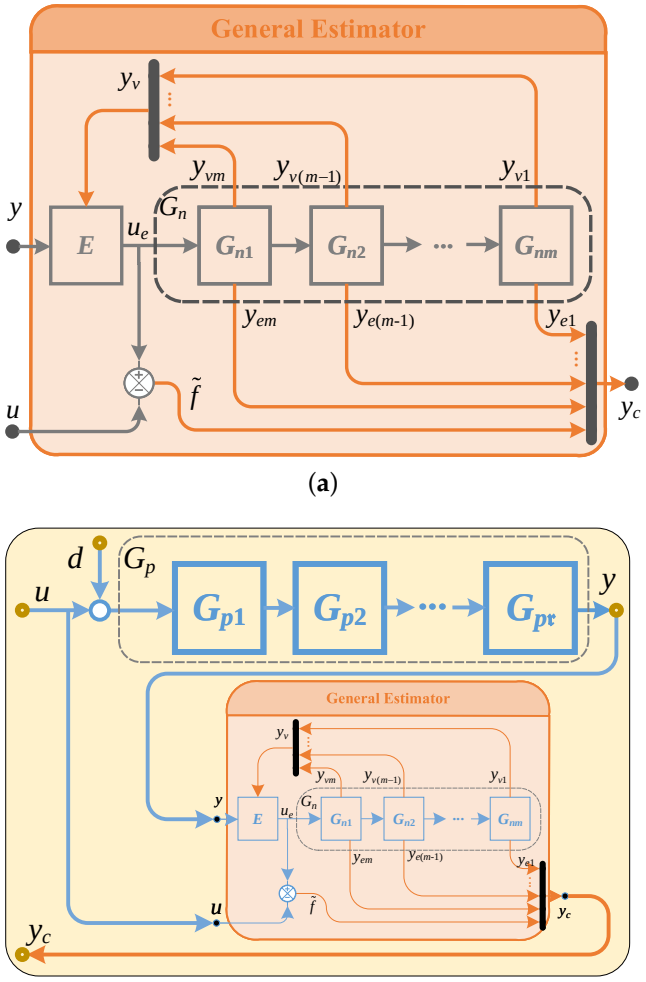


**Figure 2.** General estimator block diagrams: (**a**) the structure of the generalized inverse solver; (**b**) GIS in the closed loop.

Under (10), $G_2$ can be simplified as:

$$G_2 = \begin{pmatrix} 1 \\ s \\ s^2 \\ \vdots \\ s^{(m-2)} \\ s^{(m-1)} \end{pmatrix}_{m\times 1} G_{nm}...G_{n2}G_{n1}. \tag{11}$$

It is obvious from (8) and (11) that $y_v$ is the time derivative vector of $y_{e1}$ from order 0 up to order $m-1$.

We propose the desired dynamic equation proportional-integral-derivative (DDE PID) for the ECM $E$. Appendix A details the principle of DDE PID. The key step is the use of an integral action in (A9) and (A8) to estimate and reject the influence of $f$. Thus, $E$, transformed from (A12) and (A14), can be denoted as:

$$E = \begin{pmatrix} \underbrace{\left(P + I\frac{1}{s} - b\right)}_{E_F} & \underbrace{-\left(P + I\frac{1}{s} \quad D_1 \quad D_2 \quad \cdots \quad D_{m-1}\right)}_{E_B} \end{pmatrix}, \tag{12}$$

where the parameters are as shown in (A12).

We obtain the transfer matrices from $y$ to $y_v$ and from $y$ to $y_c$ as:

$$H_{y\mapsto y_v} = G_2(1 + E_B G_2)^{-1} E_F, \tag{13}$$

$$\begin{aligned} H_{y\mapsto y_c} &= G_1 E_F - G_1 E_B H_{y\mapsto y_v} \\ &= G_1 \underbrace{\begin{pmatrix} E_F & -E_B \end{pmatrix}}_{E} \begin{pmatrix} 1 \\ H_{y\mapsto y_v} \end{pmatrix} \\ &= G_1 E_F - G_1 E_B G_2 (1 + E_B G_2)^{-1} E_F. \end{aligned} \tag{14}$$

**Theorem 1.** *For a certain gain $l$, mentioned in Appendix A, if filter bandwidth $k \to \infty$, mentioned in Appendix A, then we have*

$$\lim_{k\to\infty} \tilde{f} = f. \tag{15}$$

**Proof.** Theorem 1 is proved in Appendix B. □

**Corollary 1.** *Under Theorem 1, we have the eigenvalue Equation (A6) of the closed-loop system $G_{cl}$ satisfying:*

$$\lim_{k\to\infty} G_{cl} = G_{des} := \frac{h_0}{h(s)}, \tag{16}$$

*where $k$ is $G_{des}$ is said to be the desired dynamics of the closed-loop system.*

**Proof.** Corollary 1 is proved in Appendix C. □

**Remark 1.** *Theorem 1 and Corollary 1 reveal that the closed-loop dynamic of GIS assigned by DDE PID will eventually approach desired dynamics $G_{des}$ with $k$ approaching infinity.*

## 4. Asymptotic Analysis

**Assumption 2.** *The functions $y_{e1}(t)$ and $y(t)$ and their time derivatives $y_{e1}^{(i)}(t)$ and $y^{(i)}(t)$ of order $i$ exist, where $i \in \mathbb{N}$ and they are continuous up to order $q$ with $t \in [t_a, t_b], t_a, t_b \geq 0, t_b > t_a$, i.e., $y_{e1}(t), y(t) \in \mathbb{C}^q[t_a, t_b]$.*

**Definition 1.** *Let $d_q^{\infty}[y_{e1}(t), y(t)]_{\varpi}$ be considered a weighted distance of order $q$ induced directly by the $L^{\infty}$ norm to measure the proximity between the two functions $y_{e1}(t)$ and $y(t)$:*

$$d_q^{\infty}[y_{e1}(t), y(t)]_{\varpi} := \sum_{i=0}^{q} \varpi_i \max_{t_a \leq t \leq t_b} \left| y_{e1}^{(i)}(t) - y^{(i)}(t) \right|, \tag{17}$$

*where $\varpi_i \geq 0$ is the weight coefficient and*

$$\varpi = \left(\varpi_0, \varpi_1, \ldots, \varpi_i, \ldots \varpi_{q-1}, \varpi_q\right)^{\top}, \tag{18}$$

*is the corresponding weight vector.*

**Remark 2.** *The distance defined by (17) is induced directly by $L^{\infty}$ norm. Another norm-induced distance, such as that induced by the $L^p$ norm, can be represented as:*

$$d_q^{p}[y_{e1}(t), y(t)]_{\varpi} := \sum_{i=0}^{q} \varpi_i \left( \int_{t_a}^{t_b} \left| y_{e1}^{(i)}(t) - y^{(i)}(t) \right|^p dt \right)^{1/p}, p \geq 1. \tag{19}$$

*It is obvious that any norm-induced distance contains the derivatives of the function, mainly as it can well-consider the oscillation of the function in the distance. Functions with small $d_0^p[y_{e1}(t), y(t)]_{\varpi}$ may greatly differ due to oscillations causing a large $d_i^p[y_{e1}(t), y(t)]_{\varpi}, i \geq 1$. $q$, $p$, and $\varpi$ can be selected according to the specific problem.*

**Definition 2.** *The set of all functions $y_{e1}(t)$, whose distance $d_q(y_{e1}(t), y(t))_\omega$ from the function $y(t)$ is less than a positive number $\delta$ in the closed interval $t \in [t_a, t_b]$, is called the $\delta$-neighborhood of function $y(t)$ in the closed interval $t \in [t_a, t_b]$, denoted by*

$$\mathbf{N}_q(\delta, y(t)) = \{y_{e1}(t) | y_{e1}(t) \in \mathbb{C}^n[t_a, t_b], d_q(y_{e1}(t), y(t))_\omega < \delta\}. \tag{20}$$

*For $y_{e1}(t) \in \mathbf{N}_q(\delta, y(t))$, $y_{e1}(t)$ and $y(t)$ are said to be with $\delta$ approach degree .*

**Assumption 3.** *$\mathbf{N}_q(\delta, y(t))$ is NOT an empty set; that is,*

$$\varnothing \subsetneqq \mathbf{N}_q(\delta, y(t)) \quad \forall \delta > 0. \tag{21}$$

*Furthermore, we assume*

$$\lim_{\delta \to 0} y_{e1}(t) = y(t) \quad \forall y_{e1}(t) \in \mathbf{N}_q(\delta, y(t)). \tag{22}$$

**Remark 3.** *Assumption 3 explains that always there is a set of tuning parameters of error-correction mechanism E that allows the output of GIS, $y_{e1}(t)$, to approach its input, $y(t)$, for a given nominal model $G_n$, combining blocks in cascade from $G_{n1}$ to $G_{nm}$.*

**Property 1.** *GIS with Definition 2 has the following properties:*

*(1)*

$$\lim_{\delta \to 0} \frac{\hat{u}_e}{\hat{y}} = G_n^{-1}. \tag{23}$$

*(2)*

$$\lim_{\delta \to 0} \frac{\hat{y}_v}{\hat{y}} = G_4. \tag{24}$$

*(3) In particular, if the nominal model of the controlled system is integral series type, i.e., $G_{n1} = G_{n2} = \ldots = G_{nm} = 1/s$, $G_4$ in (24) can be rewritten as $G_5$: that is,*

$$\lim_{\delta \to 0} \frac{\hat{y}_v}{\hat{y}} = G_5, \tag{25}$$

*where*

$$G_4 = \begin{pmatrix} 1 \\ G_{nm}^{-1} \\ G_{n(m-1)}^{-1} G_{nm}^{-1} \\ \vdots \\ G_{n3}^{-1} G_{n4}^{-1} \ldots G_{n(m-1)}^{-1} G_{nm}^{-1} \\ G_{n2}^{-1} G_{n3}^{-1} \ldots G_{n(m-1)}^{-1} G_{nm}^{-1} \end{pmatrix}_{m \times 1}, G_5 = \begin{pmatrix} 1 \\ s \\ s^2 \\ \vdots \\ s^{m-2} \\ s^{m-1} \end{pmatrix}_{m \times 1}. \tag{26}$$

**Proof.** Under Assumption 3 and if initial conditions are all zero, the Laplace transform of (22) is:

$$\lim_{\delta \to 0} \hat{y}_{e1} = \hat{y}. \tag{27}$$

Multiplying the inverse of the given nominal model and rearranging terms, we have

$$\begin{gathered} \lim_{\delta \to 0} \underbrace{(G_{nm} \ldots G_{n2} G_{n1})^{-1} \hat{y}_{e1}}_{\hat{u}_e} = \underbrace{(G_{nm} \ldots G_{n2} G_{n1})^{-1}}_{G_n^{-1}} \hat{y}, \\ \lim_{\delta \to 0} \frac{\hat{u}_e}{\hat{y}} = G_n^{-1}. \end{gathered} \tag{28}$$

Multiplying the transfer matrix $G_2$ of (28), we obtain:

$$\lim_{\delta \to 0} \frac{\overbrace{G_2 \hat{u}_e}^{\hat{y}_v}}{\hat{y}} = \underbrace{G_2 G_n^{-1}}_{G_4}, \qquad \lim_{\delta \to 0} \frac{\hat{y}_v}{\hat{y}} = G_4. \tag{29}$$

When the nominal model of the controlled system is integral series type (i.e., $G_{n1} = G_{n2} = \ldots = G_{nm} = 1/s$), $G_4$ is rewritten as $G_5$. □

**Remark 4.** *The above three propositions above explain the three functions of GIS under Assumption 3. Although they are ideal, the basic properties reveal that estimates of the inverse, intermediate variables, and derivatives can be transformed into each other.*

## 5. Desired Dynamics-Based Parameterization

Note that the principle of DDE PID is described in Appendix A. A binomial form of the desired dynamic is usually recommended:

$$G_{des} := \frac{1}{(s/\omega_e + 1)^m}, \tag{30}$$

where $\omega_e$ is the bandwidth of the desired dynamic of GIS, and $m$ is the relative order of the nominal model. An obvious relationship can be concluded from (16) and (30)

$$h_i = C_m^i \omega_e^{m-i} \equiv \frac{m!}{i!(m-i)!} \omega_e^{m-i}, \quad i = 1, 2, \ldots, m-1. \tag{31}$$

Futhermore, $k$ is the filter bandwidth mentioned in (A9). A common relation is used.

$$\gamma := \frac{\omega_e}{k} \in (0, 1]. \tag{32}$$

We propose a simple and practical method of parameterization (12) based on the desired dynamic (30) for the GIS, named desired dynamics-based GIS. The three tuning parameters of GIS: $\omega_e$, $k$, and $l$. These parameters are clear and easily tunable in engineering terms. Algorithm 1 summarizes a tuning method for GIS.

**Algorithm 1:** An algorithm to tune desired dynamic-based GIS via frequency response.

**Input:** *Cut-off frequency $\omega_{pc}$ of the plant;*
**Output:** $\omega_e$, $k$ and $l$;
***Define:*** *Specifications of tracking* [1];
***Set:*** $\gamma$ (32);
***Initialize:*** $\omega_e \leftarrow \omega_{pc}$, $l \leftarrow \mathfrak{H}$;
***Set:*** *Update of* $\omega_e$, $\Delta\omega_e$ ($\Delta\omega_e > 0$), *update of* $l$, $\Delta l$ ($l \cdot \Delta l < 0$);
**while** *Specifications* ***NOT*** *met* **do**
  **while** *Specifications* ***NOT*** *met* **do**
    *Compute the specifications;*
    *Apply update:* $l \leftarrow l + \Delta l$;
  *Apply update:* $\omega_e \leftarrow \omega_e + \Delta\omega_e$.

## 6. Stability

The system in (A2) and (A5) can be rewritten in state space form, with an error defined as $\check{f} := f - \tilde{f}$, as:

$$\dot{z} = Hz + Nr + E\check{f}, \tag{33}$$

where $z \coloneqq (z_1, z_2, \ldots, z_{\mathfrak{r}-1}, z_{\mathfrak{r}})^\top$.

$$H \coloneqq \begin{pmatrix} 0 & 1 & 0 & \cdots & 0 & 0 \\ 0 & 0 & 1 & \ddots & 0 & 0 \\ \vdots & \ddots & \ddots & \ddots & \ddots & \vdots \\ 0 & 0 & 0 & \ddots & 1 & 0 \\ 0 & 0 & 0 & \cdots & 0 & 1 \\ -h_0 & -h_1 & -h_2 & \cdots & -h_{\mathfrak{r}-2} & -h_{\mathfrak{r}-1} \end{pmatrix}, N \coloneqq \begin{pmatrix} 0 \\ 0 \\ \vdots \\ 0 \\ h_0 \end{pmatrix}, E \coloneqq \begin{pmatrix} 0 \\ 0 \\ \vdots \\ 0 \\ 1 \end{pmatrix}.$$

Note that $H$ is a Routh–Hurwitz matrix.

**Corollary 2.** *Under Theorem 1, the closed-loop of GIS assigned by DDE PID is stable.*

**Proof.** Construct a Lyapunov function of (33) with continuous first-order partial derivative, as $V(t) \coloneqq z^\top P z$, where $P$ is a positive definite matrix satisfying $H^\top P + PH \equiv -I$ and where $I$ denotes the identity matrix. Take the first derivative of $V(t)$ with respect to time and set $r \equiv 0$:

$$\begin{aligned} \dot{V}(t) &= \dot{z}^\top P z + z^\top P \dot{z} \\ &\equiv z^\top \Big( H^\top P + PH \Big) z + 2E^\top P z \check{f} \\ &= -\|z\|_2 + 2E^\top P z \check{f} \\ &\leq -\|z\|_2 + \delta \Big\| E^\top P z \Big\|_2 + \frac{\check{f}^2}{\delta}, \end{aligned} \tag{34}$$

where $\delta$ is positive. By defining two $\phi_-$ and $\phi^+$ as the minimum and maximum eigenvalues of $P$, respectively, we obtain the following.

$$0 < \phi_- \|z\|_2 \leq V(t) \leq \phi^+ \|z\|_2, \quad \|z\|_2 \neq 0, \quad \phi_- \leq \phi^+, \phi_-, \phi^+ \in \mathbb{R}^+. \tag{35}$$

It is obvious, by combining (34) and (35), that

$$\dot{V}(t) \leq -\frac{1}{\phi^+} V(t) + \frac{\delta \phi^+}{\phi_-} V(t) + \frac{\check{f}^2}{\delta}. \tag{36}$$

Let $\delta < \frac{\phi_-}{(\phi^+)^2}$ and define $K$ as

$$K \coloneqq \frac{1}{\phi^+} - \frac{\delta \phi^+}{\phi_-}. \tag{37}$$

Then, (36) can be rewritten as

$$\dot{V}(t) \leq -KV(t) + \frac{\check{f}^2}{\delta}. \tag{38}$$

Therefore, the following is true for any $t \geq t_0$.

$$V(t) \leq e^{-Kt} V(t_0) + \frac{1}{\delta} \int_{t_0}^{t} e^{-K(t-\tau)} \check{f}^2(\tau) d\tau. \tag{39}$$

Combining (35) and (39), we obtain

$$\phi_- \|z\|_2 \leq e^{-Kt} V(t_0) + \frac{1}{\delta} \int_{t_0}^{t} e^{-K(t-\tau)} \check{f}^2(\tau) d\tau. \tag{40}$$

Then, it is obvious that

$$\|z\|_2 \leq \left( \frac{V(t_0)}{\phi_-} + \frac{\int_{t_0}^{t} e^{K\tau} \breve{f}^2 d\tau}{\delta \phi_-} \right) e^{-Kt}. \tag{41}$$

Under conclusion (15) of Theorem 1, (41) is reduced to

$$\|z\|_2 \leq \frac{V(t_0)}{\phi_-} e^{-Kt}. \tag{42}$$

Consequently, GIS is stable. The proof is complete. □

## 7. Case Studies

### *7.1. Estimation Problem for Rotary Flexible Link*

We consider the system of a rotary flexible link, which abstractly represent the vibration problems of wind-turbine blades, flexible wings, solar panels, and manipulators, among others. The rotary flexible link model is shown in Figure 3a. The base of the flexible link is mounted on the load gear of the servo system. The servo angle, $\theta$, increases positively when it rotates counter-clockwise (CCW). The servo (and thus the link) turn in the CCW direction when the control voltage is positive (i.e., $V_m > 0$).

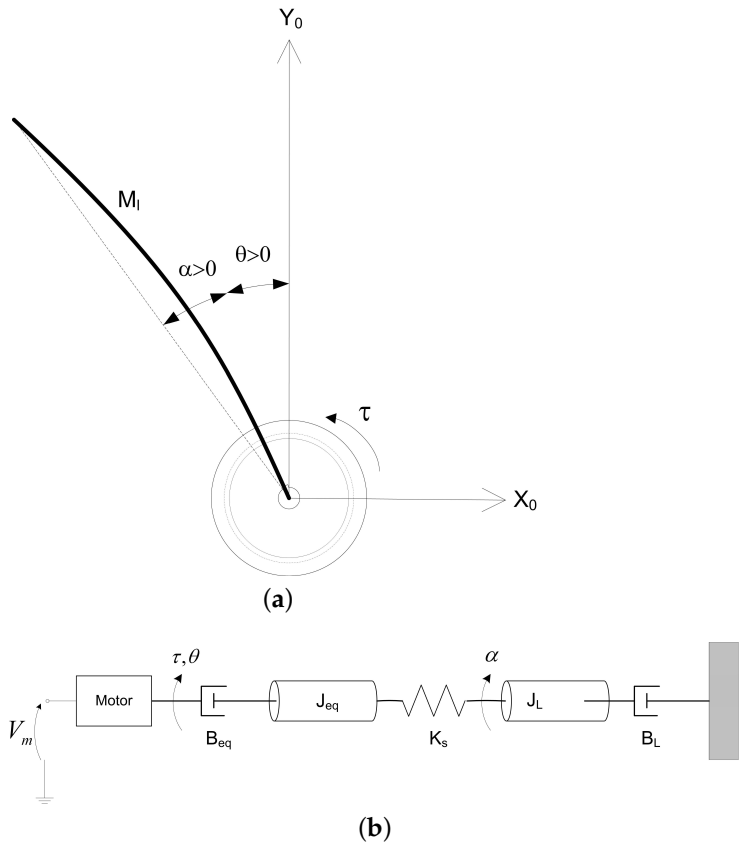


**Figure 3.** Rotary flexible link: (**a**) rotary flexible link angles; (**b**) rotary flexible link model.

The flexible link system can be represented by the diagram shown in Figure 3b. Our control variable is the input servo motor voltage, $V_m$. This generates a torque, $\tau$, at the load gear of the servo that rotates the base of the link. The viscous friction coefficient of the servo is denoted by $B_{eq}$. This is the friction that opposes the torque being applied at the servo load gear. The friction acting on the link is represented by viscous damping coefficient $B_l$. Finally, the flexible link is modeled as a linear spring with stiffness $K_s$.

**Example 1.** *The equations that describe the motions of the servo and the link with respect to the servo motor voltage (i.e., the dynamics) are obtained using the Euler–Lagrange equation:*

$$\frac{\partial^2 L}{\partial t \partial \dot{q}_i} - \frac{\partial L}{\partial q_i} = Q_i, \quad i = 1, 2. \tag{43}$$

For this system, let generalized coordinates $q_i$ be

$$q(t) \coloneqq \begin{pmatrix} q_1(t) & q_2(t) \end{pmatrix}^\top = \begin{pmatrix} \theta(t) & \alpha(t) \end{pmatrix}^\top, \tag{44}$$

where, as shown in Figure 3a, $\theta(t)$ is the servo angle, and $\alpha(t)$ is the flexible link angle. The Lagrangian of a system is defined as:

$$\begin{aligned} L \coloneqq & T - V \\ = & \underbrace{\frac{1}{2} J_{eq} \dot{\theta}^2 + \frac{1}{2} J_l (\dot{\theta} + \dot{\alpha})^2}_{T} - \underbrace{\frac{1}{2} K_s \alpha^2}_{V}, \end{aligned} \tag{45}$$

where $T$ is the total kinetic energy of the system, and $V$ is the total potential energy of the system. The generalized forces $Q_i$ are used to describe the non-conservative forces (e.g., friction) applied to a system, with respect to the generalized coordinates. In this case, the generalized force acting on the rotary arm is

$$\begin{aligned} Q \coloneqq & \begin{pmatrix} Q_1 & Q_2 \end{pmatrix}^\top \\ = & \begin{pmatrix} \tau - B_{eq} \dot{\theta} & -B_l \dot{\alpha} \end{pmatrix}^\top, \end{aligned} \tag{46}$$

where the torque applied at the base of the rotary arm (i.e., at the load gear) is generated by the servo motor, as described by the following equation:

$$\tau = \frac{\eta_g K_g \eta_m k_t \left( V_m - K_g k_m \dot{\theta} \right)}{R_m}, \tag{47}$$

where the parameters are denoted in Table 1.

**Table 1.** Description of some model parameters.

| Symbol | Description | Value | Variation |
|---|---|---|---|
| $B_{eq}$ | high-gear equivalent viscous damping coefficient | 0.015 N · m/(rad/s) | |
| $B_l$ | viscous damping coefficient | negligible | |
| $\eta_g$ | geabox efficiency | 0.90 | ±10% |
| $\eta_m$ | motor efficiency | 0.69 | ±5% |
| $J_{eq}$ | high-gear equivalent moment of inertia | 2.08 $\times 10^{-3}$ kg · m$^2$ | |
| $J_l$ | flexible link moment of inertia | 0.0038 kg · m$^2$ | |
| $K_g$ | high-gear total gear ratio | 70 | |
| | low-gear total gear ratio | 14 | |
| $K_s$ | stiffness | 1.3 N · m / rad | |
| $k_m$ | motor back-emf constant | 7.68 $\times 10^{-3}$ V/(rad/s) | ±12% |
| $k_t$ | motor current-torque constant | 7.68 $\times 10^{-3}$ N · m/A | ±12% |
| $R_m$ | motor armature resistance | 2.6 Ω | ±12% |

For Example 1, a sinusoidal input signal $V_m$ with a frequency of 10 $\pi$ rad/s and an amplitude of 50 V is acted on, while output signals $\theta$ and $\alpha$ are measured. The total duration of the simulation is 1 s, and a measurement noise with a power spectral density of 0.0005 is added at 0.5 s. GIS estimated the system dynamics under the three strategies (i.e., model-based, model-free, and semi-model-based). To be fair and convincing, the performance of GIS was tested and compared for each of these three strategies against

classical observers of equal bandwidths. The model-based observers were FSO and DOB, and the two model-free observes were HGOs and ESO. The details of these observers are provided in Table 2.

**Table 2.** Parameters of observers.

| Type | Observer | Function | | Bandwidth/(rad/s) | | Parameters |
|---|---|---|---|---|---|---|
| | | Derivatives | Disturbances | $\tau \longmapsto \theta$ | $\tau \longmapsto \alpha$ | |
| model-based | GIS[1] | √ | √ | $100\pi$ | $100\pi$ | $\gamma_\theta = 0.1$<br>$\gamma_\alpha = 0.1$<br>$l_\theta = 10$<br>$l_\alpha = -0.01$ |
| | FSO [21] | √ | | $100\pi$ | $100\pi$ | |
| | DOB [15] | | √ | | | bandwidth of the filter, $100\pi$ |
| model-free | GIS[2] | √ | √ | $100\pi$ | $100\pi$ | $\gamma_\theta = 0.1$<br>$\gamma_\alpha = 0.1$<br>$l_\theta = 10$<br>$l_\alpha = -0.01$ |
| | HGO[1] [21] | √ | | | | bandwidth of the filter, $100\pi$ |
| | HGO[2] [21] | √ | | $100\pi$ | $100\pi$ | |
| | ESO [5] | √ | √ | $100\pi$ | $100\pi$ | $\omega_{o\theta} = 1000\pi$<br>$\omega_{o\alpha} = 1000\pi$<br>$l_\theta = 10$<br>$l_\alpha = -0.01$ |
| model-weak | GIS[3] | √ | √ | $100\pi$ | $100\pi$ | $\gamma_\theta = 0.1$<br>$\gamma_\alpha = 0.1$<br>$l_\theta = 10$<br>$l_\alpha = -0.01$ |

The model-based GIS, denoted as GIS[1], corresponds to Property 1 (1) and (2), while the model-free GIS, denoted as GIS[2], corresponds to Property 1 (1) and (3). Furthermore, the semi-model-based GIS, denoted as GIS[3], was proposed to test the robustness and practicality in the engineering of GIS. Generally, GIS[3] is based on a nominal model with large variations from the controlled system. Note that the tuned parameters of GIS[3] are the same with that of GIS[1].

Figure 4a,b show comparisons of the model-based methods: GIS[1] and FSO. They present the same tracking dynamic characteristics at the same bandwidth; however, we should emphasize that GIS[1] showed better high-frequency noise suppression, especially for measured variables, $\theta$ and $\alpha$, and disturbances, $f_\theta$ and $f_\alpha$. In addition, for GIS[1], although the mathematical description of the controlled system was used as the nominal model, the specific information of the controlled system was not taken into account in the parameterization, instead, the desired dynamic-based parameterization mentioned in Section 5 was adopted. Thus, a dynamic bias in estimating the disturbance was also observed.

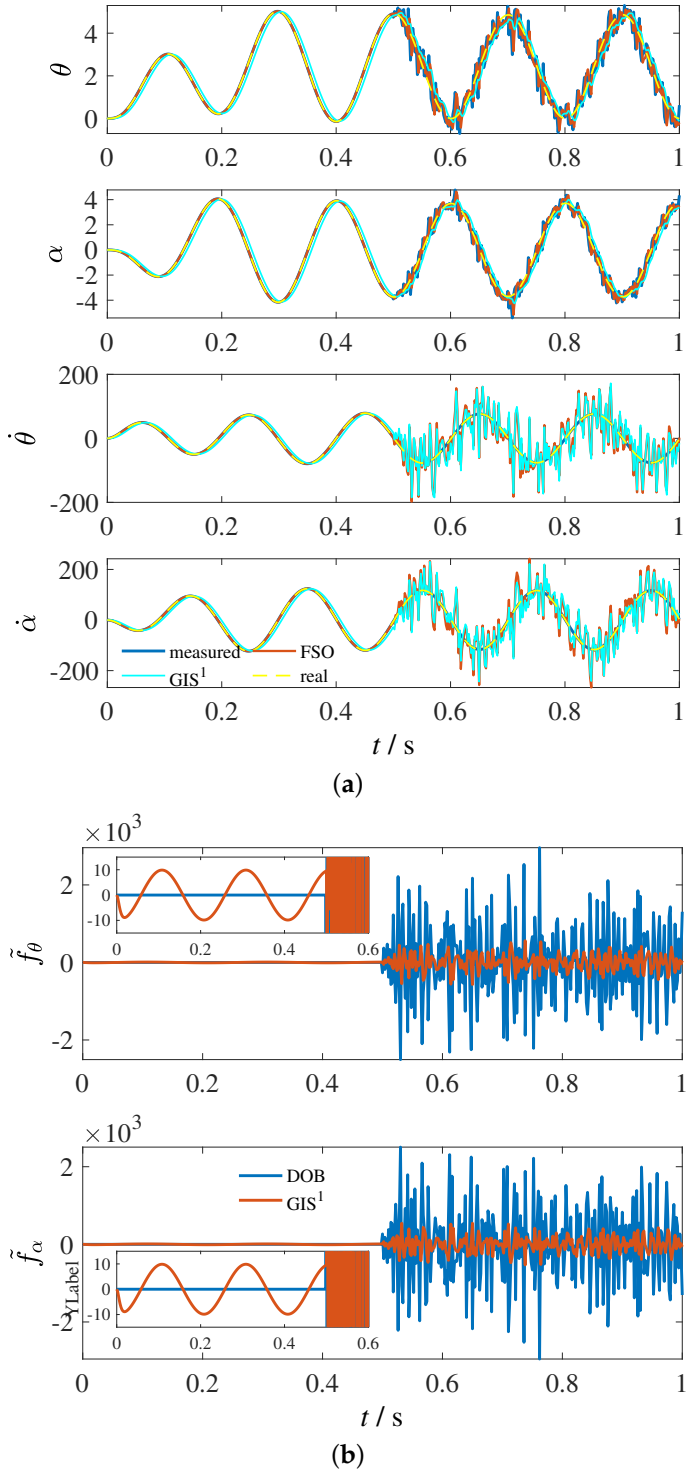


**Figure 4.** Estimated states of model-based observers: (**a**) derivatives; (**b**) disturbances.

Figure 5a,b showthe results of the model-free methods; that is, GIS$^2$, HGO$^1$, HGO$^2$, and ESO. None of these methods utilized information from the model in the design process, and they all had the same design bandwidth. It can be seen that GIS$^2$ still presented the best overall performance for the same bandwidth. More interestingly, HGO$^1$ and GIS$^2$ showed the same noise suppression performance when estimating $\theta$ and $\alpha$, while HGO$^1$ performed poorly when estimating $\dot{\theta}$ and $\dot{\alpha}$. In contrast, HGO$^2$ had the same noise suppression performance as GIS$^2$ when estimating $\dot{\theta}$ and $\dot{\alpha}$, but performed poorly when estimating $\theta$ and $\alpha$. The noise suppression performance of ESO for each variable was not

satisfactory. In terms of the disturbance estimation, GIS$^2$ was similar to the ESO, in terms of dynamic performance and noise suppression, except that ESO showed a little lag.

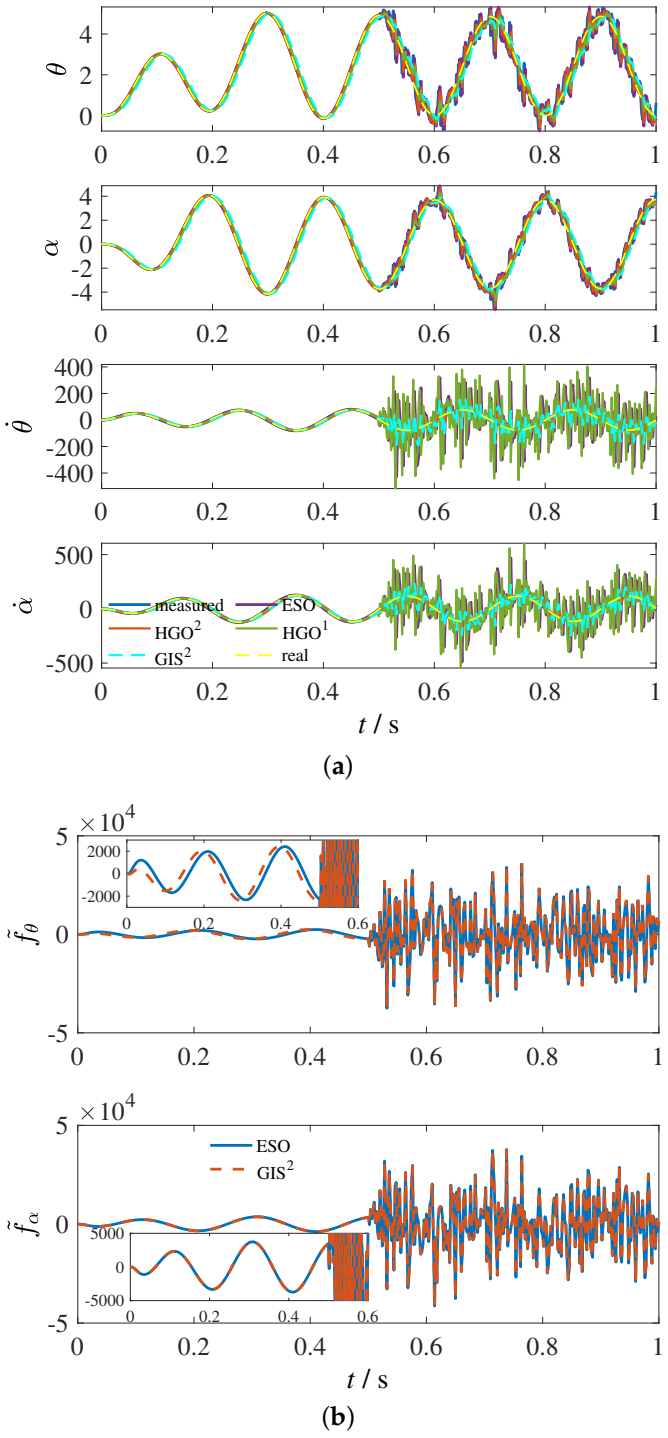


**Figure 5.** Estimated states of model-free observers: (**a**) derivatives; (**b**) disturbances.

Finally, we tested semi-model-based GIS in the condition of a nominal plant with a 100% increase in inertia. We also compared the GIS under the three estimation strategies, as shown in Figure 6a,b. An unusual conclusion is that the dynamic performance of the estimated states designed under these three strategies was almost the same. This not only demonstrates the feasibility of the GIS structure and the desired dynamic-based parameterization method, but also indicates its strong robustness and applicability. Interesting

conclusions can likewise be drawn from Figure 6b. For the three types of GISs, GIS$^2$, which did not use any information from the model, had the smallest value for the disturbance estimation, while GIS$^1$, which utilized information from the model, had the smallest value for the disturbance estimation. The result for GIS$^3$ was exactly in-between. For a given controlled system, when we know more about its dynamics, the smaller the disturbance to be estimated, the smaller the estimation burden on the estimator, and, ceteris paribus, the higher the estimation accuracy.

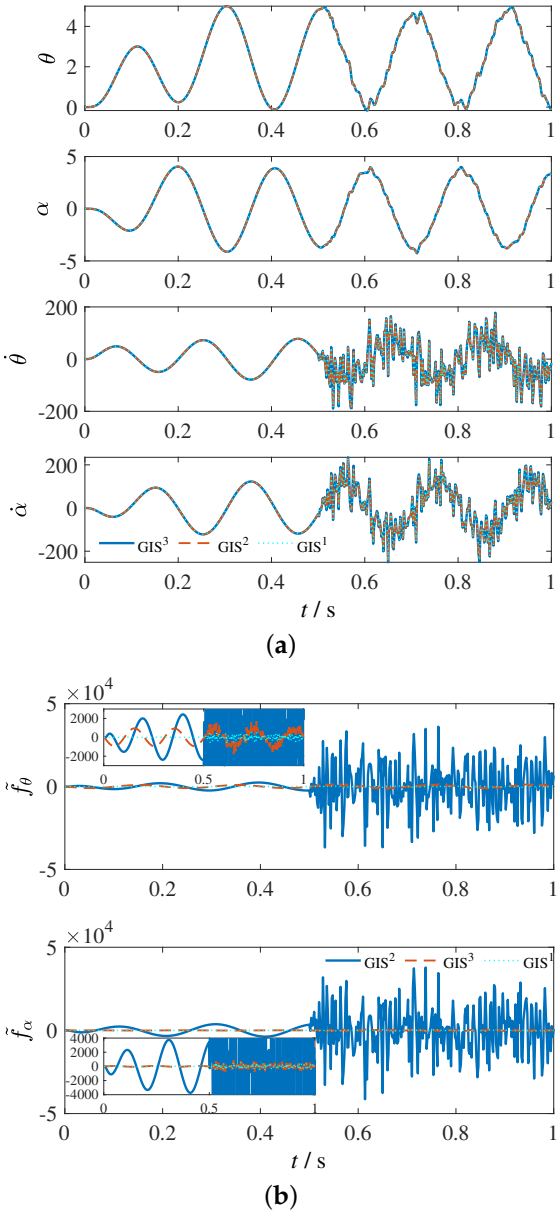


**Figure 6.** Estimated states of three types of GIS: (**a**) derivatives; (**b**) disturbances.

### *7.2. Estimation Problem in Control*

#### 7.2.1. GIS vs. DOB

When the nominal model of the controlled plant is known and there is only one nominal model (i.e., $G_n = G_{n1} = G_2$), $u_e$ becomes the estimated inverse of the model. In this case, GIS is equivalent to the DOB of the disturbance observer-based control (DOBC), and GIS can estimate the inverse of the nominal model by a simple and indirect inverse method.

We demonstrate the disturbance rejection performance in two cases—a minimum phase system and a non-minimum phase system—in order to illustrate the approximate

equivalence of DOB and GIS with the model-based approach. The design of DOBC in reference [15] considers an SISO linear minimum-phase system, with system and nominal models are given by the following.

**Example 2.**

$$G_p = \frac{s+3}{s^2+5s+4}, \tag{48a}$$

$$G_n = \frac{s+1}{s^2+2.5s+1}. \tag{48b}$$

The design and tuning principal of filter $Q(s)$ followed reference [15] where, according to the design guidelines, the filter $Q(s)$ can be selected as a first-order low-pass filter with a steady-state gain of 1; that is:

$$Q(s) = \frac{\omega_q}{s+\omega_q}, \tag{49}$$

where $\omega_q$ is the bandwidth of filter $Q(s)$. More specifically, only the disturbance estimation of DOBC (i.e., the disturbance rejection performance) is considered. For this simulation scenario, a step external disturbance $d$ was considered. Figure 7 shows that the GIS-based DOBC had the same performance as the disturbance rejection with original DOBC for a minimum phase system.

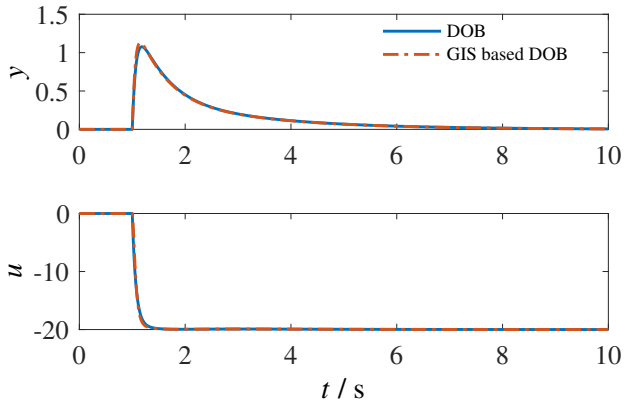


**Figure 7.** The curves of response $y$ and control output $u$ with a step external disturbance for Example 2 under DOBC and GIS-based DOBC.

**Example 3.**

$$G_p = G_n = \frac{0.8(-0.1s+1)}{(3s+1)(1.5s+1)}e^{-0.5s}, \tag{50}$$

For a non-minimum phase system, DOBC needs to divide $G_n$ into two parts: A minimum phase sub-system, $G_{n-}$, and an all-pass sub-system, $G_{n+}$. However, GIS-based DOBC requires no tedious decomposition. The simulation of Figure 8 suggests that GIS-based DOBC is also approximatly equivalent to DOBC for a non-minimum phase system.

$$G_{n+} = \frac{-0.1s+1}{0.1s+1}e^{-0.5s}, \tag{51a}$$

$$G_{n-} = \frac{0.8(0.1s+1)}{(3s+1)(1.5s+1)}, \tag{51b}$$

$$Q = \frac{k}{s+k}. \tag{52}$$

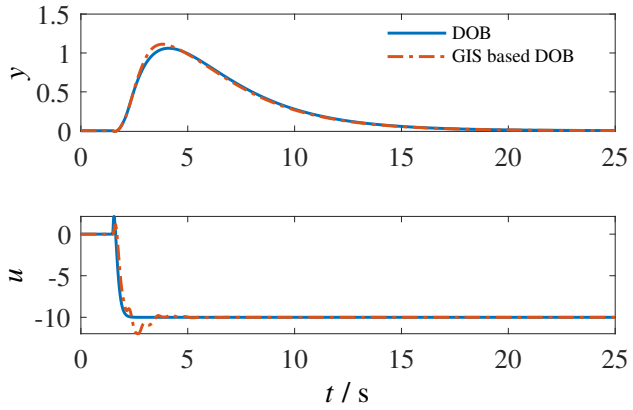


**Figure 8.** The curves of response $y$ and control output $u$ with a step external disturbance for Example 3 under DOBC and GIS-based DOBC.

7.2.2. GIS vs. ESO

Nest, we considered the case where the nominal model of the controlled system is a double integral series type ( $G_{n1} = b_0/s$ and $G_{n2} = 1/s$). In this case, GIS is equivalent to the ESO of ADRC. $y_{e2}$ and $u_e$ are the estimated derivative information of the integral series. GIS realizes estimation of the derivatives and total disturbance. The control, which replaces ESO in ADRC with GIS, is denoted GIS-based ADRC.

We demonstrate the performance of the disturbance rejection in a second-order system to illustrate the equivalence of ADRC and GIS-based ADRC. The system and nominal models are given by the following.

**Example 4.**

$$G_p = \frac{1}{(1+s)(1+0.2s)}. \tag{53}$$

For this case, the tracking and disturbance rejection performance was compared. In this simulation scenario, a unit step of set-point from 0 to 1 was added at time 0, and a lumped step perturbation occured at time 3. Figure 9 shows that the GIS-based ADRC presented the same performance as ADRC, in terms of both tracking and disturbance rejection.

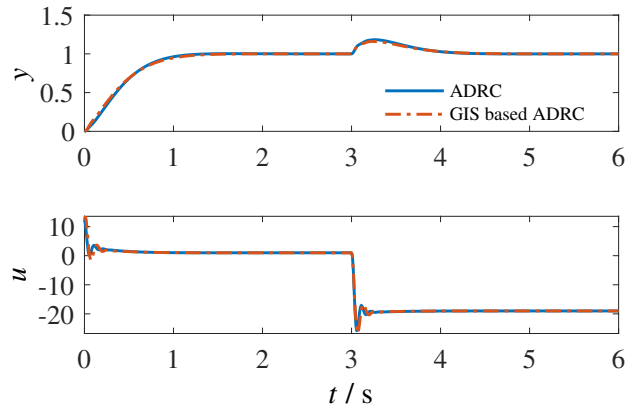


**Figure 9.** The curves of response $y$ and control output $u$ with a unit step of set-point and a centralized step disturbance for the Example 4 under ADRC and GIS-based ADRC.

## 8. Discussion

In this paper, we proposed a novel estimator, called the generalized inverse solver (GIS) and a matching desired dynamics-based parameterization method. GIS is an estimator which is similar to a closed-loop system, structurally consisting of nominal models and an error-correction mechanism (ECM). Specifically, the nominal model can be model-

based, semi-model-based, or even model-free, depending on prior knowledge of the model information. In addition,we designed a pole placement for the ECM of GIS based on desired dynamics-based parameterization, where states are directly used in ECM to accelerate the convergence of GIS. The dynamics of GIS are assigned by the desired dynamic equation proportional-integral-derivative (DDE PID) control, which eventually tunes the dynamics of GIS to a more standardized desired dynamics by following a simple rule. In addition, GIS builds a bridge structurally through which the functional transformation between different observers can be realized. Its fundamentals, asymptotic properties, and convergence were discussed. Furthermore, a rotary flexible link was simulated with GIS. Different estimation methods were compared with GIS under the same design bandwidth, indicating that GIS can greatly improve the noise suppression performance with little loss of dynamic estimation performance. Moreover, different GISs can be designed according to the amount of prior knowledge of the system. The dynamic estimation performance of the different GIS approaches was almost the same, illustrating the strong robustness of GISs (although by means of the uniform design method). Finally, some control cases were studied, including a comparison with DOB and ESO to illustrate their approximate equivalence to GIS.

GIS is simple and easy to tune. In the paper, we mainly discussed its basic characteristics. Its frequency characteristics and time domain representation remain to be further investigated. In addition, the form of the desired dynamics can be more diversified. For example, a combination of non-linear algebraic equations and linear dynamic equations can be introduced to describe the desired dynamic. More meaningfully, the case studies in this paper are mainly linear systems. The issues of control for different plants (especially nonlinear systems) and different constraints, thus deserve further exploration.

**Author Contributions:** Conceptualization, D.L. and S.L.; methodology, D.L. and S.L.; software, S.L.; validation, S.L. and Y.Z.; formal analysis, S.L. and Y.Z.; investigation, S.L.; resources, S.L.; data curation, S.L.; writing—original draft preparation, S.L.; writing—review and editing, S.L., Y.Z., Z.G., Y.C., D.L. and M.Z.; visualization, S.L.; supervision, Z.G., Y.C., D.L. and M.Z.; project administration, D.L. and M.Z.; funding acquisition, D.L. and M.Z. All authors have read and agreed to the published version of the manuscript.

**Funding:** This research was funded by the National Science and Technology Major Project (J2019-III-0020-0064) of China and the National Natural Science Foundation of China with Grant/Award No. 62103044.

**Institutional Review Board Statement:** Not applicable.

**Informed Consent Statement:** Not applicable.

**Data Availability Statement:** Not applicable.

**Conflicts of Interest:** The authors declare no conflicts of interest.

## Abbreviations

The following abbreviations are used in this manuscript:

| | |
|---|---|
| DDE PID | Desired Dynamic Equation proportional-integral-derivative; |
| DOB | Disturbance observer; |
| DOBC | Disturbance observer-based control; |
| ECM | Error-correction mechanism; |
| ESO | Extended state observer; |
| FSO | Full-state observer; |
| GIS | Generalized inverse solver; |
| HGO | High-gain observer; |
| KF | Kalman filter; |
| LO | Luenberger observer. |

## Appendix A. The Principle of DDE PID

**Assumption A1.**

*(1) The relative degree* $\mathfrak{r}$ *is known.*
*(2) The spectrum of the polynomial* $\beta(s)$ *is in the open left half-plane.*
*(3) The sign* $\sigma(\mathfrak{H})$ *of the high frequencies gain* $\mathfrak{H}$ *is known.*
*(4) The measure of the output variable* $y(t)$ *and of its time derivatives* $y^{(i)}(t)$ *of order i is available up to order* $\mathfrak{r}-1$.

The normal form of the system (2) can be obtained by defining the following new coordinates.

$$\begin{aligned} z_i &:= CA^{i-1}x, \quad i = 1, \ldots, \mathfrak{r}, \\ w_i &:= x_i, \quad i = 1, \ldots, \mathfrak{n}-\mathfrak{r}. \end{aligned} \tag{A1}$$

In the new coordinates (A1), we obtain the system in the normal form, which has the following structure.

$$\begin{aligned} \dot{z}_i &= z_{i+1}, \quad i = 1, \ldots, \mathfrak{r}-1, \\ \dot{z}_{\mathfrak{r}} &= -\sum_{i=0}^{\mathfrak{r}-1} c_i z_{i+1} - \sum_{i=0}^{\mathfrak{n}-\mathfrak{r}-1} d_i w_{i+1} + \mathfrak{H}u, \\ \dot{w}_i &= w_{i+1}, \quad i = 1, \ldots, \mathfrak{n}-\mathfrak{r}-1, \\ \dot{w}_{\mathfrak{n}-\mathfrak{r}} &= -\sum_{i=0}^{\mathfrak{n}-\mathfrak{r}-1} b_i w_{i+1} z_1, \\ y &= z_1. \end{aligned} \tag{A2}$$

The equation describing the dynamics of $\dot{z}_{\mathfrak{r}}$ can be rewritten as follows:

$$\dot{z}_{\mathfrak{r}} = f(z_1, \ldots, z_{\mathfrak{r}}, w_1, \ldots, w_{\mathfrak{n}-\mathfrak{r}}, u) + lu, \tag{A3}$$

$$f(z_1, \ldots, z_{\mathfrak{r}}, w_1, \ldots, w_{\mathfrak{n}-\mathfrak{r}}, u) := -\sum_{i=0}^{\mathfrak{r}-1} c_i z_{i+1} - \sum_{i=0}^{\mathfrak{n}-\mathfrak{r}-1} d_i w_{i+1} + (\mathfrak{H}-l)u, \tag{A4}$$

where $l$ is an estimate of $\mathfrak{H}$ and $\sigma(l) \equiv \sigma(\mathfrak{H})$.

**Assumption A2.** *The state vector is measurable and the values of coefficients* $c_i, i = 0, \ldots, \mathfrak{r}-1, d_i, i = 0, \ldots, \mathfrak{n}-\mathfrak{r}-1$, *and* $\mathfrak{H}$ *are known, i.e.,* $l \equiv \mathfrak{H}$.

Under Assumption A2, a possible control law for the tracking of (A2) is as follows:

$$\begin{aligned} u :=& \frac{1}{l}\left(h_0 r - \sum_{i=0}^{\mathfrak{r}-1} h_i z_{i+1} - f\right) \\ =& \frac{1}{l}\left(h_0 r - \sum_{i=0}^{\mathfrak{r}-1} h_i z_{i+1} + \sum_{i=0}^{\mathfrak{r}-1} c_i z_{i+1} + \sum_{i=0}^{\mathfrak{n}-\mathfrak{r}-1} d_i w_{i+1}\right). \end{aligned} \tag{A5}$$

where $r$ is a reference signal for the tracking and $h_i, i = 0, 1, \ldots, \mathfrak{r}-1$, are suitable positive constants. Equation (A5) guarantees that the eigenvalues of the closed-loop system (A2) and (A5) coincide with the roots of $h(s)$ and $\beta(s)$, with the following being the case.

$$h(s) := h_0 + h_1 s + \cdots + h_{\mathfrak{r}-1} s^{\mathfrak{r}-1} + s^{\mathfrak{r}} \equiv \sum_{i=0}^{\mathfrak{r}} h_i s^i, \quad h_{\mathfrak{r}} \equiv 1. \tag{A6}$$

Substituting (A5) into (A3) yields a desired dynamic:

$$\frac{y_{\hat{des}}}{\hat{r}} = G_{des}(s) := \frac{h_0}{h(s)}. \tag{A7}$$

As Assumption A2 may not hold in reality, the control law (A5) cannot be actually implemented. A possible way to overcome this difficulty is the use of an integral action to reject the influence of term $f$, as in the following proportional-integral-derivative (PID) control law, which is proposed here for the stabilization of (A2):

$$u := \frac{1}{l}\left(h_0 r - \sum_{i=0}^{\mathfrak{r}-1} h_i z_{i+1} - \tilde{f}\right), \tag{A8}$$

where

$$\begin{aligned} \tilde{f} &= \xi + k z_{\mathfrak{r}}, \\ \dot{\xi} &= -k\xi - k^2 z_{\mathfrak{r}} - klu. \end{aligned} \tag{A9}$$

where $k$ is a filter bandwidth. Substituting (A9) to (A8), we obtain the following.

$$\dot{\xi} = -k\left(h_0 r - \sum_{i=0}^{\mathfrak{r}-1} h_i z_{i+1}\right). \tag{A10}$$

Integrate both sides of (A10), it is obvious that

$$\xi = -k\left(h_0 \int (r - z_1)dt - \sum_{i=1}^{\mathfrak{r}-1} h_i z_i\right). \tag{A11}$$

Combined with (A11), (A8) can be rewritten as follows:

$$\begin{aligned} u =& \frac{k\left(h_0 \int (r - z_1)dt - \sum_{i=1}^{\mathfrak{r}-1} h_i z_i - z_{\mathfrak{r}}\right)}{l} + \frac{\left(h_0(r - z_1) - \sum_{i=1}^{\mathfrak{r}-1} h_i z_{i+1}\right)}{l} \\ \equiv& \underbrace{\frac{h_0 + kh_1}{l}}_{P} e + \underbrace{\frac{kh_0}{l}}_{I} \int e dt - \sum_{i=1}^{\mathfrak{r}-1} \left(\underbrace{\frac{h_i + kh_{i+1}}{l}}_{D_i} z_{i+1}\right) - \underbrace{\frac{kh_1}{l}}_{b} r, \quad h_{\mathfrak{r}} \equiv 1 \\ =& Pe + I \int e dt - \sum_{i=1}^{\mathfrak{r}-1} D_i z_{i+1} - br, \end{aligned} \tag{A12}$$

where $e := r - z_1$ and

$$\begin{cases} P = \dfrac{h_0 + kh_1}{l}, \\ I = \dfrac{kh_0}{l}, \\ D_i = \dfrac{h_i + kh_{i+1}}{l}, \quad h_{\mathfrak{r}} \equiv 1, \quad i = 1, 2, \ldots, \mathfrak{r} - 1, \\ b = \dfrac{kh_1}{l}. \end{cases} \tag{A13}$$

As the goal is to approach the desired dynamic (A7) by estimate $\tilde{f}$ in (A9), the control law denoted as (A12) is called a control method of the desired dynamic equation PID (DDE PID). Particular, if $\mathfrak{r}$ equals 2, which means that the process can be regarded as a general second-order system, the parameters of DDE PID can be evaluated as follows.

$$\begin{cases} P = \dfrac{h_0 + kh_1}{l}, \\ I = \dfrac{kh_0}{l}, \\ D = \dfrac{h_1 + k}{l}, \\ b = \dfrac{kh_1}{l}. \end{cases} \tag{A14}$$

## Appendix B. The Proof of Theorem 1

**Proof.** The Laplace transform of (A9) is denoted as follows.

$$\begin{aligned} \hat{\tilde{f}} &= \hat{\xi} + k\hat{z}_{\mathfrak{r}}, \\ s\hat{\xi} &= -k\hat{\xi} - k^2\hat{z}_{\mathfrak{r}} - kl\hat{u}. \end{aligned} \tag{A15}$$

Substituting the second equation into the first one and merging terms, we obtain the following.

$$\hat{\tilde{f}} = \frac{k}{s+k}\left(\hat{z}_{\mathfrak{r}} - l\hat{u}\right). \tag{A16}$$

Combined with (A3), (A16) is rewritten as follows.

$$\hat{\tilde{f}} = \frac{k}{s+k} f. \tag{A17}$$

Taking the limit of $k$ on both sides of (A17), we obtain the following.

$$\begin{aligned} \lim_{k\to\infty} \tilde{f} &= \lim_{k\to\infty} \frac{k}{s+k} f \\ &= f. \end{aligned} \tag{A18}$$

The proof is complete. □

## Appendix C. The proof of Corollary 1

**Proof.** Substituting (A8) into (A3), we obtain the following.

$$\dot{z}_{\mathfrak{r}} + \sum_{i=0}^{\mathfrak{r}-1} h_i z_{i+1} = h_0 r + \left(f - \tilde{f}\right). \tag{A19}$$

Taking the Laplace transform of (A19) and rearranging the terms yields the following.

$$\frac{\hat{y}}{\hat{r}} = \frac{1}{h(s)\hat{r}}\left(\hat{f} - \hat{\tilde{f}}\right) + G_{des}. \tag{A20}$$

Taking the limit of $k$ on both sides of (A20) yields the following.

$$\lim_{k\to\infty} \frac{\hat{y}}{\hat{r}} = \lim_{k\to\infty} \left( \frac{1}{h(s)\hat{r}}\left(\hat{f} - \hat{\tilde{f}}\right) + G_{des} \right). \tag{A21}$$

Under the conclusion (A18) of Theorem 1, (A21) is reduced to the following.

$$\begin{aligned} \lim_{k\to\infty} \frac{\hat{y}}{\hat{r}} &= \lim_{k\to\infty} G_{des} \\ &= G_{des}. \end{aligned} \tag{A22}$$

The proof is complete. □

## References


1. Bernard, P.; Andrieu, V.; Astolfi, D. Observer design for continuous-time dynamical systems br. *Annu. Rev. Control.* **2022**, *53*, 224–248. [CrossRef]
2. Chen, G.; Liu, S.J.; Tang, Z.G.; Xu, J.T.; Wang, W.Z. A novel method of multiple adaptive notch filtering for flexible missile vibration suppression. *Aircr. Eng. Aerosp. Technol.* **2020**, *92*, 1149–1157. [CrossRef]
3. Luenberger, D.G. Observing the state of a linear system. *IEEE Trans. Mil. Electron.* **1964**, *8*, 74–80. [CrossRef]
4. Sariyildiz, E.; Ohnishi, K. A guide to design disturbance observer. *J. Dyn. Syst. Meas. Control. Trans. ASME* **2014**, *136*, 021011. [CrossRef]
5. Gao, Z. Scaling and Bandwidth-Parameterization based Controller Tuning. In Proceedings of the 2003 American Control Conference, Milwaukee, WI, USA, 27–29 June 2003; pp. 4989–4996.
6. Guo, B.Z.; Han, J.Q.; Xi, F.B. Linear tracking-differentiator and application to online estimation of the frequency of a sinusoidal signal with random noise perturbation. *Int. J. Syst. Sci.* **2002**, *33*, 351–358. [CrossRef]
7. Guo, B.Z.; Zhao, Z.L. On convergence of tracking differentiator. *Int. J. Control.* **2011**, *84*, 693–701. [CrossRef]
8. Luenberger, D.G. Observers For Multivariable Systems. *IEEE Trans. Autom. Control* **1966**, *11*, 190–197. [CrossRef]
9. Luenberger, D.G. Introduction to Observers. *IEEE Trans. Autom. Control* **1971**, *16*, 596–602. [CrossRef]
10. Jo, N.H.; Seo, J.H. Input output linearization approach to state observer design for nonlinear system. *IEEE Trans. Autom. Control* **2000**, *45*, 2388–2393. [CrossRef]
11. Mahony, R.; van Goor, P.; Hamel, T. Observer Design for Nonlinear Systems with Equivariance. *Annu. Rev. Control. Robot. Auton. Syst.* **2022**, *5*, 221–252. [CrossRef]
12. Yang, J.; Gao, Z.; Li, Z.; Qian, W. An improved multiple-state observer of Boolean control networks. *Asian J. Control* **2019**, *21*, 2651–2661. [CrossRef]
13. Zhang, Z.; Leifeld, T.; Zhang, P. Reduced-Order Observer Design for Boolean Control Networks. *IEEE Trans. Autom. Control* **2020**, *65*, 434–441. [CrossRef]
14. Xiang, Q.; Yang, Q.; Wu, Z.H. Observer design and stability analysis for a class of PDE chaotic systems. *J. Frankl.-Inst.-Eng. Appl. Math.* **2021**, *358*, 3232–3257. [CrossRef]
15. Li, S.; Yang, J.; Chen, W.H.; Chen, X. *Disturbance Observer-Based Control: Methods and Applications*; CRC Press: Boca Raton, FL, USA, 2014.
16. Chen, W.H.; Yang, J.; Guo, L.; Li, S. Disturbance-Observer-Based Control and Related Methods - An Overview. *IEEE Trans. Ind. Electron.* **2016**, *63*, 1083–1095. [CrossRef]
17. Liu, S.; Zhang, Y.L.; Xue, W.; Shi, G.; Zhu, M.; Li, D. Frequency response-based decoupling tuning for feedforward compensation ADRC of distributed parameter systems. *Control. Eng. Pract.* **2022**, *126*, 105265. [CrossRef]
18. Liu, S.; Shi, G.; Li, D. Active disturbance rejection control based on feedforward inverse system for turbofan engines. In Proceedings of the 6th IFAC Conference on Engine Powertrain Control, Simulation and Modeling E-COSM 2021, Tokyo, Japan, 23–25 August 2021; pp. 376–381.
19. Efimov, D.V.; Fridman, L. A Hybrid Robust Non-Homogeneous Finite-Time Differentiator. *IEEE Trans. Autom. Control.* **2011**, *56*, 1213–1219. [CrossRef]
20. Cruz-Zavala, E.; Moreno, J.A. Levant's Arbitrary-Order Exact Differentiator: A Lyapunov Approach. *IEEE Trans. Autom. Control.* **2019**, *64*, 3034–3039. [CrossRef]
21. Wang, W.W.; Gao, Z.Q.; Aac, A.A.C. A comparison study of advanced state observer design techniques. In Proceedings of the Annual American Control Conference (ACC 2003), Milwaukee, WI, USA, 27–29 June 2003; pp. 4754–4759.
22. Yang, F.; Wei, C.Z.; Wu, R.; Cui, N.G. Non-Recursive Fixed-Time Convergence Observer and Extended State Observer. *IEEE Access* **2018**, *6*, 62339–62351. [CrossRef]
23. Hong, J.; Laflamme, S.; Dodson, J.; Joyce, B. Introduction to State Estimation of High-Rate System Dynamics. *Sensors* **2018**, *18*, 217. [CrossRef]
24. Phuong, T.T.; Ohishi, K.; Mitsantisuk, C.; Yokokura, Y.; Ohnishi, K.; Oboe, R.; Sabanovic, A. Disturbance Observer and Kalman Filter Based Motion Control Realization. *IEEJ J. Ind. Appl.* **2018**, *7*, 1–14. [CrossRef]
25. Hua, C.C.; Wang, K.; Chen, J.N.; You, X. Tracking differentiator and extended state observer-based nonsingular fast terminal sliding mode attitude control for a quadrotor. *Nonlinear Dyn.* **2018**, *94*, 343–354. [CrossRef]
26. Liao, K.; Xu, Y.; Zhou, H. A robust damping controller for DFIG based on variable-gain sliding mode and Kalman filter disturbance observer. *Int. J. Electr. Power Energy Syst.* **2019**, *107*, 569–576. [CrossRef]
27. Abro, G.E.M.; Asirvadam, V.S.; Zulkifli, S.A.B.; Sattar, A.; Kumar, D.; Anwer, A. Effects of unmodelled dynamic factors on an under-actuated quadrotor: A review of hybrid observer design methods. *Meas. Control.* **2020**, *53*, 1978–1987. [CrossRef]
28. Ghapani, F.; Babadi, B. Two parameter weighted mixed estimator in linear measurement error models. In *Communications in Statistics-Simulation and Computation*; Taylor & Francis: Abingdon, UK, 2020; p. 11.
29. Tornambè, A.; Valigi, P. A decentralized controller for the robust stabilization of a class of MIMO linear systems. *Syst. Control Lett.* **1992**, *18*, 383–390. [CrossRef]
30. Wang, W.; Li, D.; Gao, Q.; Wang, C. Two-degrees-of-freedom PID controller tuning method. *Qinghua Daxue Xuebao/J. Tsinghua Univ.* **2008**, *48*, 1962–1966.

31. Shi, G.; Wu, Z.; Liu, S.; Li, D.; Ding, Y.; Liu, S. Research on the Desired Dynamic Selection of a Reference Model-Based PID Controller: A Case Study on a High-Pressure Heater in a 600 MW Power Plant. *Processes* **2022**, *10*, 1059. [CrossRef]
32. Shi, G.; Liu, S.; Li, D.; Ding, Y.; Chen, Y. A Controller Synthesis Method to Achieve Independent Reference Tracking Performance and Disturbance Rejection Performance. *ACS Omega* **2022**, *7*, 16164–16186. [CrossRef]